Hidden chiral symmetry protected $\mathbb{Z}\oplus\mathbb{Z}$ topological insulators in a ladder dimer model

Jin-Yu Zou[1] and Bang-Gui Liu[1,*]

[1] *Beijing National Laboratory for Condensed Matter Physics, Institute of Physics, Chinese Academy of Sciences, Beijing 100190, China.*

(Dated: June 23, 2015)

We construct a two-leg ladder dimer model by using two orbitals instead of one in Su-Schrieffer-Heeger (SSH) dimer chain and find out a chiral symmetry in it. In this model, the otherwise-hidden additional chiral symmetry allows us to define two chiral massless fermions and show that there exist interesting topological states characterized by $\mathbb{Z}\oplus\mathbb{Z}$ and corresponding zero mode edge states. Our complete phase diagram reveals that there is an anomalous topologically nontrivial region in addition to the normal one similar to that of SSH model. The anomalous region features that the inter-cell hopping constants can be much smaller than the intra-cell ones, being opposite to the normal region, and the zero mode edge states do not have well-defined parity each. Finally, we suggest that this ladder dimer model can be realized in double-well optical lattices, ladder polymer systems, and adatom double chains on semiconductor surfaces.

The discovery of quantum Hall effect in two-dimensional electron gas opens a new era in physics[1–3]. In such systems, topology is involved in their electronic phases and phase transitions. In 2005 Kane *et al* [4, 5] discovered the time-reversal-invariant topological phase in graphene with spin-orbit interaction, causing a boom in researching topological insulator[6–12]. Since topological insulators can be classified according to their symmetries[13], whether an insulating system is a topological insulator or not is dependent on the symmetries of its crystalline and electronic structures. Fortunately, optical lattices engineered with interfering laser beams allow us to study specific interesting models which cannot be easily found in nature[14]. Such models can possess novel configurations with potentials of single or multiple periods. Controls of atoms in the s and p orbitals in optical lattices can exhibit many exotic quantum states[15–19], including topological nontrivial states. For instance, there is a topological insulator phase in an s-p-orbital ladder reduced from a two-dimensional double-well optical lattice[20] and a topological semimetal in fermionic optical lattice[21].

Simple dimer chain, also known as Su-Schrieffer-Heeger (SSH) model, is a simple but important model to show typical topological property of one-dimensional systems[22, 23], although it was originally proposed to describe one-dimensional polyacetylene[24]. The simple dimer chain belongs to BDI class according to its symmetry[13], and is characterized by the topological invariant $C\in\mathbb{Z}$.

Here, we construct a two-orbital dimer model, or a ladder dimer model, which can be realized by optical lattices similar to those with s and p orbitals[15, 20, 21]. We find that the ladder dimer model can possess higher symmetry than the dimer chain and thus have richer topological phases, beyond BDI class, and can be characterized by topological invariant $C\in\mathbb{Z}\oplus\mathbb{Z}$. We plot the complete phase diagram and work out its zero-mode edge states. Furthermore, we find out the relationship between this ladder dimer model and massless chiral fermion. More detailed results will be presented in the following.

Results

Model and symmetry. We construct a general two-leg ladder dimer model by using two orbitals instead of one in the simple SSH dimer model. Presented in Fig. 1 is a schematic of the ladder dimer model. Its Hamiltonian can be defined as

$$\begin{aligned}H=&\sum_j t_s(a^\dagger_{jBs}a_{jAs}+h.c.)+t'_s(a^\dagger_{jBs}a_{j+1,As}+h.c.)\\&+t_p(a^\dagger_{jBp}a_{jAp}+h.c.)+t'_p(a^\dagger_{jBp}a_{j+1,Ap}+h.c.)\\&+t_1(a^\dagger_{jBp}a_{jAs}+h.c.)+t'_1(a^\dagger_{jBp}a_{j+1,As}+h.c.)\\&+t_2(a^\dagger_{jBs}a_{jAp}+h.c.)+t'_2(a^\dagger_{jBs}a_{j+1,Ap}+h.c.)\end{aligned}\tag{1}$$

where the fermion operators a_{iPq} and $a^\dagger_{iPq}$ ($P=A$ and B, and $q=s$ and p_x) are used to define the model. Because we are considering s and p_x orbitals, with the x axis being along the chain, the real-space symmetry of the wave functions implies that the nearest-neighbor hybridization and hopping can be nonzero and the onsite hybridization of the two orbitals needs to be zero. In addition, no next-nearest-neighbor hopping is considered to keep high symmetry, which is consistent with the SSH dimer model. Defining $\hat{C}^\dagger_j=[a^\dagger_{jAs},a^\dagger_{jBs},a^\dagger_{jAp},a^\dagger_{jBp}]$, we make a Fourier transformation under periodic boundary condition, and obtain $\hat{C}^\dagger_k=\frac{1}{\sqrt{L}}\sum_j C^\dagger_j e^{ikaj}=[a^\dagger_{kAs},a^\dagger_{kBs},a^\dagger_{kAp},a^\dagger_{kBp}]$, where L is the number of the unit cells. As a result, the Hamiltonian can be simplified into $H=\sum_k \hat{C}^\dagger_k H_k \hat{C}_k$

* Corresponding author: bgliu@iphy.ac.cn

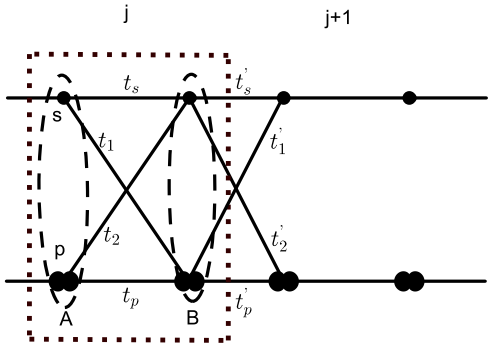

FIG. 1. A schematic of the ladder dimer model with the hopping parameters shown.

with H_k being expressed as

$$H_k = \begin{pmatrix} 0 & t_s + t_s' e^{-ika} & 0 & t_1 + t_1' e^{-ika} \\ t_s + t_s' e^{ika} & 0 & t_2 + t_2' e^{ika} & 0 \\ 0 & t_2 + t_2' e^{-ika} & 0 & t_p + t_p' e^{-ika} \\ t_1 + t_1' e^{ika} & 0 & t_p + t_p' e^{ika} & 0 \end{pmatrix} \tag{2}$$

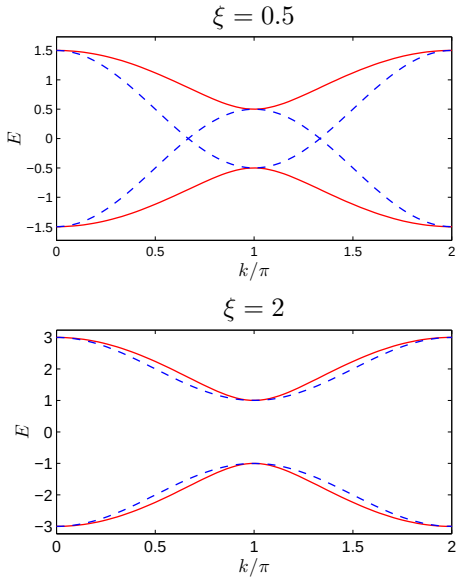

FIG. 2. The reduced energy spectra of $E = \pm\sqrt{(\xi + \cos k)^2 + \sin^2 k}$ with $\xi = 0.5$ (upper panel) and $\xi = 2$ (lower panel), in comparison with the curves described with function $E = \pm(\xi + \cos k)$.

Using two sets of Pauli matrices, $\overrightarrow{\tau} = (\tau_x, \tau_y, \tau_z)$ in the sp orbital space and $\overrightarrow{\sigma} = (\sigma_x, \sigma_y, \sigma_z)$ in the AB subspace, we can express the Hamiltonian in a compact form. Because we are considering real parameters, there should be some relationships among the parameters[15, 20, 21]. If we let the p_x orbitals be in an order like antiferromagnetic order[15], we can have $t_1 = t_2 = \delta$ and $t_1' = t_2' = \delta'$ for an optical lattice. As a result, the Hamiltonian can be simplified as

$$\begin{aligned} H_k^a =& I \otimes [(t + t' \cos ka)\sigma_x + t' \sin ka \sigma_y] \\ &+ \tau_z \otimes [(\tau + \tau' \cos ka)\sigma_x + \tau' \sin ka \sigma_y] \\ &+ \tau_x \otimes [(\delta + \delta' \cos ka)\sigma_x + \delta' \sin ka \sigma_y] \end{aligned} \tag{3}$$

where $t = (t_s + t_p)/2$, $t' = (t_s' + t_p')/2$, $\tau = (t_s - t_p)/2$, and $\tau' = (t_s' - t_p')/2$. Each of the these parameters can be nonzero. Consequently, this model has time reversal symmetry ($T = K$), particle-hole symmetry ($C = I \otimes \sigma_z K$), chiral symmetry ($S = I \otimes \sigma_z$), and space inversion symmetry ($R = I \otimes \sigma_x$). It belongs to the BDI class and is characterized by $\mathbb{Z}$.

Introducing the unitary transformation defined by $U = \exp(-i\alpha\tau_y/2) \otimes I$, we change H_k^a into the following hamiltonian.

$$\begin{aligned} \mathcal{H}_k^s =& U^\dagger H_k^a U = (t + t' \cos ka) I \otimes \sigma_x + t' \sin ka I \otimes \sigma_y \\ &+ [(w + w' \cos ka)\tau_z \otimes \sigma_x + w' \sin ka \tau_z \otimes \sigma_y] \end{aligned} \tag{4}$$

where $w = \delta/\sin\alpha$ and $w' = \delta'/\sin\alpha$, and α (in $[0, \pi]$) is determined by $\tan\alpha = \delta/\tau = \delta'/\tau'$. Here, the condition $\delta/\tau = \delta'/\tau'$ is required in the diagonalization of the τ space, which reduces one freedom in the parameter space, but fortunately, we have only four freedoms in $\mathcal{H}_k^s$, two less than those in $\mathcal{H}_k^a$. This parameter condition can be satisfied by requiring $\delta/\delta' = \tau/\tau' = (t_s - t_p)/(t_s' - t_p')$ in $\mathcal{H}_k^a$. It is easy to prove that this hamiltonian commutes with $P = \tau_z \otimes I$, $[\mathcal{H}_k^s, P] = 0$. Therefore, we have found a hidden chiral symmetry in H_k^s. It should be pointed out that the hidden chiral symmetry is guaranteed by both the inversion symmetry and the parameter condition. With this additional P chiral symmetry, the hamiltonian can be viewed as massless fermions and we have four additional symmetries: $T' = PT$, $C' = PC$, $S' = PS$, and $R' = PR$. Then, we can introduce the projection operators

$$P_L = \frac{1}{2}(I + \tau_z) \otimes I, P_R = \frac{1}{2}(I - \tau_z) \otimes I \tag{5}$$

and write the hamiltonian as a block-diagonal form

$$\mathcal{H}_k^s = \begin{pmatrix} H_L^s(k) & 0 \\ 0 & H_R^s(k) \end{pmatrix} \tag{6}$$

where the $H_L^s = [(t + w) + (t' + w')\cos ka]\sigma_x + (t' + w')\sin ka\sigma_y$ and $H_R^s = [(t - w) + (t' - w')\cos ka]\sigma_x + (t' - w')\sin ka\sigma_y$ describe the left and right chiral fermions, respectively. Each of $H_L^s(k)$ and $H_R^s(k)$ has two independent parameters, and therefore they are independent of each other.

Topological states and phase diagram. Diagonalizing the hamiltonians H_L and H_R, we obtain the energy

$$E_\gamma = \pm\sqrt{\Delta_1^2 + \Delta_2^2}, \tag{7}$$

where $\gamma = (L, R)$, $\Delta_1 = (t' \pm w')\sin ka$, $\Delta_2 = (t \pm w) + (t' \pm w')\cos ka$, and the minus sign corresponds to the

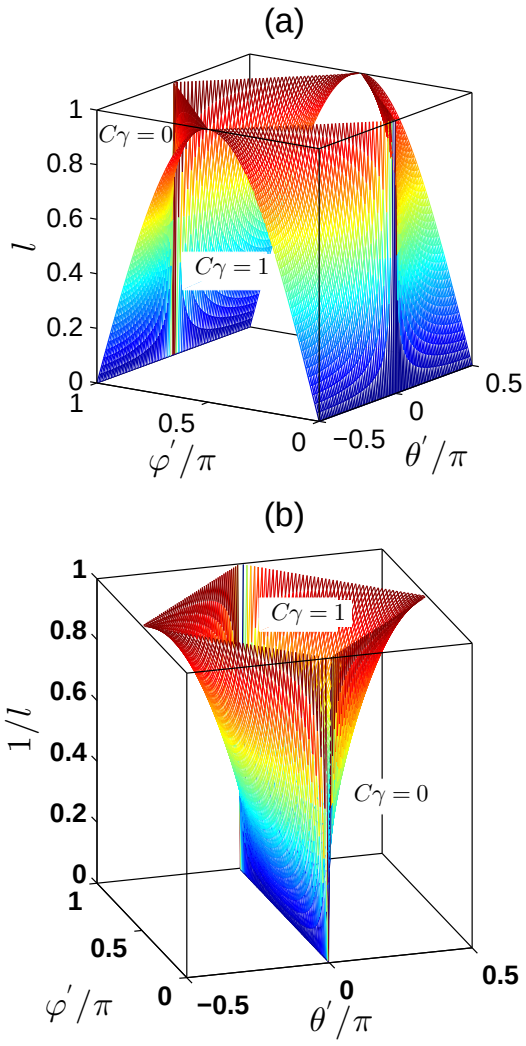

FIG. 3. The (l,θ',φ') phase diagram for $l|\sin(\theta')|/|\sin(\varphi')| < 1$ for $l = r/r' < 1$ (a) and $1/l = r'/r < 1$ (b). The true (l,θ,φ) diagram is determined by $l|\sin(\theta+\pi/4)/\sin(\varphi+\pi/4)| < 1$ for the left and $l|\sin(\theta-\pi/4)/\sin(\varphi-\pi/4)| < 1$ for the right, with $0 \le l < +\infty$. Because of the absolute value sign, the complete phase diagram can be plotted in terms of $\theta \in [-\pi/2, \pi/2]$ and $\varphi \in [0, \pi]$.

left and plus the right. The energy band structure of the left part becomes gapless if we have $|\frac{t+w}{t'+w'}| = 1$, and for the right part the condition is $|\frac{t-w}{t'-w'}| = 1$. Each of the two parts is a dimer chain. We present in Figure 2 a reduced form of E_γ, $E = \pm\sqrt{(\xi+\cos k)^2 + \sin^2 k}$, with $\xi = \xi_L = (t+w)/(t'+w')$ for the left part and $\xi = \xi_R = (t-w)/(t'-w')$ for the right one. It is easy to see the energy structure inversion in the figure.

For the hamiltonian $H_\gamma(k) = \vec{h}_\gamma(k) \cdot \vec{\sigma}$ here, the winding number of vector $\vec{h}_\gamma(k)$ is a good approach to topological characterization because there is no σ_z component[26, 27], $\vec{h}_\gamma(k) = \rho_\gamma(k)(\cos\phi_\gamma(k), \sin\phi_\gamma(k), 0)$. The winding number can be expressed as

$$C_\gamma = \frac{1}{2\pi}\oint \phi'_\gamma(k)dk = \frac{\Delta\phi_\gamma}{2\pi} \tag{8}$$

It should be pointed out that our C_γ here is equivalent to either zero or +1, and the value -1 does not appear because we have the same coefficients for $\sin ka$ and $\cos ka$ in $H_\gamma(k)$, which is different from a generalized SSH chain model[28]. The total winding number is equivalent to $C = C_L \oplus C_R$. This definition is well defined because it is gauge invariant. Under this definition, the left and right parts enter nontrivial topological states respectively if the following conditions are satisfied.

$$\begin{cases} |\xi_L| = |\dfrac{t+w}{t'+w'}| < 1, & \text{for the left} \\ |\xi_R| = |\dfrac{t-w}{t'-w'}| < 1, & \text{for the right} \end{cases} \tag{9}$$

Generally speaking, the two parts become trivial or nontrivial independently, and therefore the topological invariant belongs to $\mathbb{Z} \oplus \mathbb{Z}$.

The original four parameters, namely t, w, t', and w', are not convenient to describing the topological phase diagram effectively. Instead, we use r, r', θ, and φ in terms of the definition: $t = r\sin\theta$, $w = r\cos\theta$, $t' = r'\sin\varphi$, and $w' = r'\cos\varphi$. Because $t' = w' = 0$ means that the model is trivial, we can assume $r' > 0$ and $r \ge 0$. The conditions (9) of the nontrivial topological states are equivalent to

$$l|\frac{\sin(\theta+\pi/4)}{\sin(\varphi+\pi/4)}| < 1 \quad \text{or} \quad l|\frac{\sin(\theta-\pi/4)}{\sin(\varphi-\pi/4)}| < 1. \tag{10}$$

where $l = r/r'$. The sign of absolute value guarantees that the period is π for both θ and φ. For brevity, we show a (l,θ',φ') phase diagram for $l|\frac{\sin(\theta')}{\sin(\varphi')}| < 1$ in Figure 3. We have two phases with $C_\gamma = 0$ and $C_\gamma = 1$ for θ'. The true phase diagram of the left part can be obtained by replacing θ' with $\theta + \pi/4$, and that of the right part with $\theta - \pi/4$. The whole phase diagram consists of four phases with $C = (0\oplus 0)$, $(0\oplus 1)$, $(1\oplus 0)$, and $(1\oplus 1)$. It can be proved that there is no $C = (0\oplus 0)$ phase for $l < 1$ and no $C = (1\oplus 1)$ phase for $l > 1$. It should be pointed out that the $(0\oplus 1)$ phase is topologically different from the $(1\oplus 0)$ phase. This is because $H^s_L(k)$ is independent of $H^s_R(k)$ in $\mathcal{H}^s_k$. Furthermore, it can be proved that there exist a pair of zero mode edge states at the interface between the $(1\oplus 0)$ phase of $(\xi_L,\xi_R)=(\xi_1,1/\xi_1)$ and the $(0\oplus 1)$ phase of $(\xi_L,\xi_R)=(1/\xi_1,\xi_1)$, where $\xi_1 < 1$ is assumed. Therefore, the four phases are topologically different from each other.

It is interesting to compare this phase diagram with the conventional dimer model. Here r describes the hopping parameter within the unit cell, and r' between the unit cells. The conventional dimer chain is topologically nontrivial when and only when the hopping within the unit cell is smaller than the hopping between the unit

cells. In contrast, our ladder dimer model can be topologically nontrivial even when r is larger than r'. Furthermore, we find that for $r < r'$, the left and right parts can be topologically nontrivial at the same time, but for $r > r'$, they will never be topologically nontrivial simultaneously. These happen because for each of the two parts the hopping terms are determined by two independent parameter freedoms (not independent parameters).

Zero mode edge states. To explicitly elucidate the nontrivial topological states, we study the band structures and explore edge states under open boundary condition. As unveiled by Delplace *et al*[26], under the open boundary condition, a finite single chain with L_c dimers possess two edge states located at the two ends when $v/v' < 1 - 1/(L_c + 1)$, where v is the intra-cell hopping parameter and v' the inter-cell one. For the ladder dimer model, the conditions of edge states are $l|\frac{t+w}{t'+w'}| < 1 - \frac{1}{L_c+1}$ for the left and $l|\frac{t-w}{t'-w'}| < 1 - \frac{1}{L_c+1}$ for the right. In long chain limit of L_c approaching to ∞, these edge-state conditions are consistent with bulk conditions for nontrivial topological states. For arbitrary finite L_c, we define $l' = l/[1 - 1/(L_c + 1)]$ and obtain the conditions for the existence of the zero mode edge states,

$$l'|\frac{\sin(\theta + \pi/4)}{\sin(\varphi + \pi/4)}| < 1 \quad \text{or} \quad l'|\frac{\sin(\theta - \pi/4)}{\sin(\varphi - \pi/4)}| < 1, \qquad (11)$$

which takes the same form as the bulk conditions in Eq. (10). Therefore, the phase diagram of the zero mode edge states can be obtained by substituting l' for l in Eq. (10) and Figure 3. This makes a clear correspondence between the bulk nontrivial topological states and the zero mode edge states. It should be pointed out that there is a special region determined by $\frac{1}{l'} < |\frac{\sin(\theta \pm \pi/4)}{\sin(\varphi \pm \pi/4)}| < \frac{1}{l}$ near the phase boundary, in which there is no zero mode edge state but there exist bulk nontrivial topological states. The zero mode edge states will appear in pair because we have two edges. For $l' > 1$, there can be a pair of zero mode edge states in some (θ,φ) region and there is not any edge state in the remaining region. For $l' < 1$, there are either one or two pairs of zero mode edge states for given (θ,φ) values. The difference between l and l' can be attributed to different finite size effect under the open boundary condition from that under the periodic boundary condition.

In order to show the edge states more clearly, we present in Figure 4 the energy levels as functions of the parameter φ with given parameters of $L_c = 20$, $r = 1$, $r' = 2$, and $\theta = \frac{5}{12}\pi$. Here, because of $l = 1/2$ and $l' = 21/40$, it can be inferred from Eqs. (10) and (11) that at least one of the two parts are topologically nontrivial, and there are either 2 or 1 pairs of zero mode edge states. For the φ values near both $\varphi = +\pi/4$ and $-\pi/4$, there are one pair of zero mode edge states with opposite parity. In contrast, there are two pairs of zero mode edge states near $\varphi = 0$, with one pair of them belonging to the left part and the others to the right part. Each of these edge states has well-defined parity. The transition points are determined by $|\sin(\varphi \pm \pi/4)| > \sqrt{3}l'/2 = 21\sqrt{3}/80$.

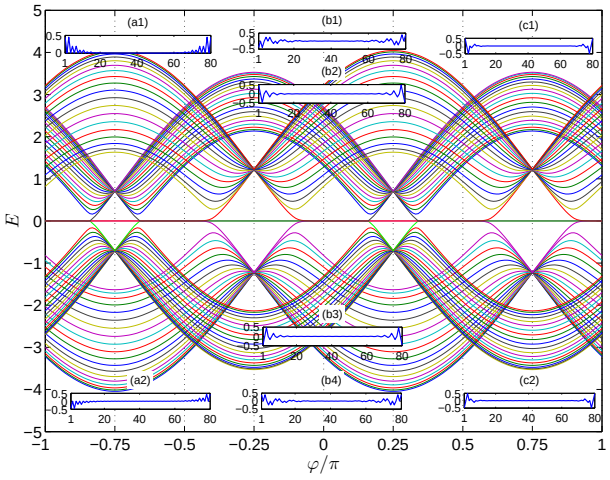

FIG. 4. The energy levels as functions of the parameter φ with $L_c = 20$, $r = 1$, $r' = 2$, and $\theta = 5\pi/12$. At least one of the two parts is topologically nontrivial because of $l = 1/2$ and $l' = 21/40$. The inserts (a1) and (a2) are the two zero mode edge states for $\varphi = \pi/4$ ($-3\pi/4$ also), corresponding to the nontrivial right part. The inserts (c1) and (c2) are the two edge states for $\varphi = -\pi/4$ ($3\pi/4$ also), corresponding to the nontrivial left part. The (b1-b4) shows the four edge states for $\varphi = 0$ ($\pm\pi/2$ and $\pm\pi$ also), which corresponds to the situation in which both of the two parts are topologically nontrivial. The edge states have well-defined parity and appear in pair.

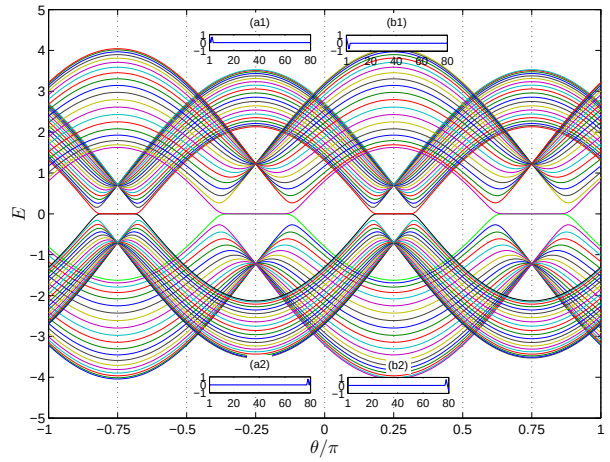

FIG. 5. The energy levels as functions of the parameter θ with $L_c = 20$, $r = 2$, $r' = 1$, and $\varphi = 5\pi/12$. In this case of $l = 2$ and $l' = 21/10$, at most one of the two parts can be nontrivial. The inserts (a1) and (a2) are the two zero mode edge states for $\theta = -\pi/4$ ($3\pi/4$ also), corresponding to the nontrivial right part. The inserts (b1) and (b2) are the two edge states for $\varphi = \pi/4$ ($-3\pi/4$ also), corresponding to the nontrivial left part. The edge states appear in pair and have no defined parity.

Presented in Figure 5 are the energy levels as functions of the parameter θ with $L_c = 20$, $r = 2$, $r' = 1$, and $\varphi = \frac{5}{12}\pi$. In this case, we have $l = 2$ and $l' = 21/10$, and there are at most one pair of zero mode edge states

according to Eq. (12). It is clear in Figure 5 that there is no edge state near $\theta = 0$ and equivalent points, and there are one pair of zero mode edge states near $\theta = \mp\pi/4$ and equivalent points. Because being degenerate in energy, they have no well-defined parity, in contrast to those in the case of $l' < 1$. The transition points are determined by $|\sin(\theta \pm \pi/4)| < 1/(2l') = 5/21$. The two edge states can be transformed into each other by the space inversion.

Discussion

Zak phases. In addition to the winding number, the Zak phase can be used to characterize the ladder dimer model. The Zak phase for γ (L,R) can be defined as

$$\Phi_Z^\gamma = i \oint dp \langle u_q^\gamma | \partial_q u_q^\gamma \rangle, \tag{12}$$

where the $|u_q^\gamma\rangle$ are the Bloch wave functions, with γ being both L and R. For such one-dimensional models, Φ_Z^γ is defined up to 2π due to the gauge transformation. For each of L and R, the Zak phase is quantized so that $\Phi_Z^\gamma = 0,\ \pi$ Mod$[2\pi]$, because of the inversion symmetry. Such Zak phase has been measured in the case of simple SSH model[29]. Defining $Z_\gamma = \Phi_Z^\gamma/\pi$, we have $Z_\gamma = 0$ and 1 accordingly. It can be proved in terms of definitions (8) and (12) and the gauge invariance that Z_γ is equivalent to C_γ. As a result, we can also use the Zak phases to characterize the topological phases of the model.

High chiral symmetry and $\mathbb{Z} \oplus \mathbb{Z}$ uniqueness. At first sight there would be many high-symmetry ladder dimer models from the SSH dimer mode, but actually it is not the case. First of all, both the on-site hybridization and the next-nearest-neighbor hopping needs to be forbidden to keep the T, C, S, and R symmetries and the hidden chiral symmetry P. This requires that any vertical rung is absent in Fig. 1, in contrast with multi-leg extension with vertical rungs[26]. In addition, there is a restrictive parameter condition between the inter-orbital and the intra-orbital hopping parameters. The hidden chiral symmetry is necessary to the additional T', C', S', and R' symmetries and the resultant $\mathbb{Z} \oplus \mathbb{Z}$ topological insulators in the ladder dimer model. The two conditions for nontrivial topological phases in the ladder dimer model, $\xi_L < 1$ for the left part and $\xi_R < 1$ for the right in (9), are each similar to that in the SSH dimer model. The unitary transformation U allows one more parameter freedom in the original hamiltonian H_k^a. Actually, one cannot achieve higher chiral symmetry in such two-leg ladder dimer model from the SSH model. Therefore, in this sense, our ladder dimer model possessing the high chiral symmetry (including the hidden chiral symmetry) and the $\mathbb{Z} \oplus \mathbb{Z}$ topological insulator phases is unique up to a unitary transformation.

Experimental realization. Now we address how to realize the ladder dimer model in (1). Inspired by earlier work[15, 20], we propose to realize the one-dimensional model with a two-orbital optical lattice with the optical potential given by

$$\begin{aligned} V(x,y) = V_{x1}\sin^2 kx + V_{x2}\sin^2(2kx + \frac{\pi}{2}) \\ + V_{y1}\sin^2 ky + V_{y2}\sin^2(2ky + \frac{\phi}{2}), \end{aligned} \tag{13}$$

where we keep $V_{y1,2} \gg V_{x1,2}$. This optical lattice has a double-well structure in the y direction and causes the particles to transit alternately between the sub-wells with two different tunneling barriers (B_1 and B_2) in the x direction. The tunneling barrier between the two wells in the y direction is much larger than B_1 and B_2 in the x direction. Consequently, the low-energy physics of the two-dimensional system (13) reduces to a two-leg ladder model with alternate barriers between sub-wells in the x direction. We can control parameters ϕ and $V_{y1,2}$ to tune the well depth of the two legs, and change $V_{x1,2}$ to tune the depth of the sub-wells in each leg. Letting the s orbital of the upper leg have the same energy as the p_x orbital of the lower leg, we realize the ladder dimer model showed in Fig. 1 and defined in Eq. (1) by filling the low-lying levels of the relevant s and p_x orbitals with a single species of fermions[15, 20]. Making the p_x orbitals be in an order like antiferromagnetic order[15], we can obtain $t_1 = t_2 = \delta$ and $t_1' = t_2' = \delta'$ and simplify the Hamiltonian (1) into Eq. (3). In addition, this model should be realized in ladder polymer systems or adatom double chains on appropriate semiconductor surfaces.

Conclusion. In summary, we have constructed a ladder dimer model with higher symmetry, defined in Eq. (3), than the usual SSH dimer chain model. In this case, there is a hidden chiral symmetry between the two orbitals that allows us to define two chiral massless fermions. Furthermore, we show that the ladder dimer model can exhibit interesting topological states characterized by $\mathbb{Z} \oplus \mathbb{Z}$ and have zero mode edge states, assuming a one-dimensional $\mathbb{Z} \oplus \mathbb{Z}$ topological insulator. We find out complete phase diagram for the bulk topological states and zero mode edge states. Importantly, the phase diagram reveals that there exist nontrivial topological states in not only the normal region with $r' \geq r$ but also the anomalous region with $r' < r$, where r' is the inter-cell hopping constant and r the intra-cell one, in contrast with the usual dimer chain model which shows nontrivial topological states only in the $r' \geq r$ region. We also find that the zero mode edge states have well-defined parity in the normal region, but do not in the anomalous region. Finally, we suggest that this ladder dimer model can be realized in double-well optical lattices, ladder polymer systems, and adatom double chains on semiconductor surfaces.

[1] Klitzing, K. V., Dorda, G. & Pepper, M. New Method for High-Accuracy Determination of the Fine-Structure Constant Based on Quantized Hall Resistance. *Phys. Rev. Lett.* **45**, 494 (1980).

[2] Tsui, D. C., Stormer, H. L. & Gossard, A. C. Two-Dimensional Magnetotransport in the Extreme Quantum Limit. *Phys. Rev. Lett.* **48**, 1559 (1982).

[3] Thouless, D. J., Kohmoto, M., Nightingale, M. P. & den Nijs, M. Quantized Hall Conductance in a Two-Dimensional Periodic Potential. *Phys. Rev. Lett.* **49**, 405 (1982).

[4] Kane, C. L. & Mele, E. J. Z2 Topological Order and the Quantum Spin Hall Effect. *Phys. Rev. Lett.* **95**, 146802 (2005).

[5] Kane, C. L. & Mele, E. J. Quantum spin Hall effect in graphene. *Phys. Rev. Lett.* **95**, 226801 (2005).

[6] Bernevig, B. A., Hughes, T. A. & Zhang, S. C. Quantum Spin Hall Effect and Topological Phase Transition in HgTe Quantum Wells. *Science* **314**, 1757 (2006).

[7] Fu, L. & Kane, C. L., Time reversal polarization and a Z2 adiabatic spin pump. *Phys. Rev. B* **74**, 195312 (2006).

[8] Fu, L., Kane, C. L., & Mele, E. J. Topological Insulators in Three Dimensions. *Phys. Rev. Lett.* **98**, 106803 (2007).

[9] Moore, J. E. & Balents, L. Topological invariants of time-reversal-invariant band structures. *Phys. Rev. B* **75**, 121306(R) (2007).

[10] Zhang, H., Liu, C. X., Qi, X. L., Dai, X., Fang, Z. & Zhang, S. C. Topological insulators in Bi2Se3, Bi2Te3 and Sb2Te3 with a single Dirac cone on the surface. *Nat. Phys.* **5**, 438 (2009).

[11] Hasan, M. Z. & Kane, C. L. Topological insulators, *Rev. Mod. Phys.* **82**, 3045 (2010)

[12] Qi, X. L. & Zhang, S. C. Topological insulators and superconductors, *Rev. Mod. Phys.* **83**, 1057 (2011).

[13] Schnyder, A. P., Ryu, S., Furusaki, A. & Ludwig, A. W. W. Classification of topological insulators and superconductors in three spatial dimensions, *Phys. Rev. B* **78**, 195125 (2008).

[14] Bloch, I. Quantum coherence and entanglement with ultracold atoms in optical lattices. *Nature* **453**, 1016-1022 (2008).

[15] Wirth, G., Olschlager, M., & Hemmerich, A. Evidence for orbital superfluidity in the P-band of a bipartite optical square lattice. *Nat. Phys.* **7**, 147 (2011).

[16] Soltan-Panahi, P., Luhmann, D. S., Struck, J., Windpassinger, P. & Sengstock, K. Quantum phase transition to unconventional multi-orbital superfluidity in optical lattices. *Nat. Phys.* **8**, 71 (2012).

[17] Tarruell, L., Greif, D., Uehlinger, T., Jotzu, G. & Esslinger, T. Creating, moving and merging Dirac points with a Fermi gas in a tunable honeycomb lattice. *Nature* **483**, 302 (2012).

[18] Zhou, Q., Porto, J. V. & das Sarma, S. Condensates induced by interband coupling in a double-well lattice. *Phys. Rev. B* **83**, 195106 (2011).

[19] Cai, Z. & Wu, C. Complex and real unconventional Bose-Einstein condensations in high orbital bands. *Phys. Rev. A* **84**, 033635 (2011).

[20] Li, X., Zhao, E. & Liu, W. V. Topological states in a ladder-like optical lattice containing ultracold atoms in higher orbital bands, *Nat. Commun.* **4**, 1523 (2013).

[21] Sun, K., Liu, W. V., Hemmerich, A. & Sarma, S. D. Topological semimetal in a fermionic optical lattice, *Nat. Phys.* **8**, 67 (2012).

[22] Ryu, S., Schnyder, A. P., Furusaki, A. & Ludwig, A. W. W. Topological insulators and superconductors: tenfold way and dimensional hierarchy, *New J. Phys.* **12**, 065010 (2010).

[23] Altland, A., & Zirnbauer, M. R. Nonstandard symmetry classes in mesoscopic normal-superconducting hybrid structures, *Phys. Rev. B* **55**, 1142 (1997).

[24] Su, W. P., Schrieffer, J. R. & Heeger, A. J. Solitons in Polyaeetylene, *Phys. Rev. Lett.* **42**, 1698 (1979).

[25] Chiu, C. K., Yao, H. & Ryu, S. Classification of topological insulators and superconductors in the presence of reflicion symmetry, *Phys. Rev. B* **88**, 075142 (2013).

[26] Delplace, P., Ullmo, D. & Montambaux, G. Zak phase and the existence of edge states in graphene. *Phys. Rev. B* **84**, 195452 (2011).

[27] Ryu, S. & Hatsugai, Y. Topological origin of zero energy edge states in particle hole symmetric system, *Phys. Rev. Lett.* **89**, 077002 (2002).

[28] Li, L.-H., Xu, Z.-H. & Chen, S. Topological phases of generalized Su-Schrieffer-Heeger models. *Phys. Rev. B* **89**, 085111 (2014).

[29] Atala, M., Aidelsburger, M., Barreiro, J. T., Abanin, D., Kitagawa, T. Demler, E. & Bloch, I. Direct measurement of the Zak phase in topological Bloch bands, *Nat. Phys.* **9**, 795 (2013)

Acknowledgments

This work is supported by Nature Science Foundation of China (Grant No. 11174359), by Chinese Department of Science and Technology (Grant No. 2012CB932302), and by the Strategic Priority Research Program of the Chinese Academy of Sciences (Grant No. XDB07000000).

Author contributions

BGL supervises the project. JYZ did all the derivation. Both carried out the analysis and wrote the manuscript.

Additional information

Competing financial interests: The authors declare no competing financial interests.